Vol. 19, No. 3 (2020) 1255-1264
Revista Mexicana de Ingeniería Química

Erosion behavior of 440C stainless steel cryogenically treated

Comportamiento bajo la erosión del acero inoxidable 440C tratado criogénicamente

J. Ibarra[1]*, E. Rodríguez[2], M.A. González[3], S. López Cuenca[1], A. Medina[4], G.I. Vásquez[2]

[1]*Instituto Tecnológico José Mario Molina Pasquel y Henríquez, Camino Arenero No. 1101, Col. El Bajío, C.P. 45019, Zapopan, Jalisco, México.*
[2]*Universidad de Guadalajara, Departamento de Ingeniería de Proyectos, José Guadalupe Zuno # 48, Zapopan, Jalisco, México.*
[3]*CONACyT-Universidad de Guadalajara, CUCEI, Ciudad Universitaria, Blvd. Marcelino García Barragán 1421, Guadalajara, Jalisco C.P 44430, México*
[4]*UMSNH. Instituto de Investigación en Metalurgia y Materiales. Edificio U. Ciudad Universitaria. Morelia Michoacán México C. P. 58000*

Received: November 13, 2019; Accepted: January 11, 2020

Abstract

The quality of most of metallic products depends on its superficial condition and how it deteriorates in operation; mostly the type of deterioration phenomena is the principal factor which affects life time and operation performance of machines components. The erosion is one of the most deteriorating factors which metals are exposed to. In the present work, erosion by solid particle tests of martensitic 440C stainless steel were realized. Silica sand (SiO_2) was used as erodent (is the most commonly occurring natural abrasive contaminant, constituting about 60% of the earth,s crust), at four impact angles and four impact speed of the particles. Graphs of erosion show a brittle behavior tendency. To determine roughness and the maximum erosion depth, a 3D mapping of the eroded surface was done, showing that there is no correspondence between the angle of maximum mass loss and the angle at which maximum penetration marks were observed at 5 and 10 psi flow pressure. Scanning electron microscopy was used to determine the erosion mechanisms for each impact angle test. These results are compared to similar studies in which the behavior under the erosion is different, (in this paper the maximum erosion is observed at 60° angle and in other researches the maximum erosion is observed at 30° angle).

Keywords: 440C stainless steel, erosion, silica sand SiO_2, impact angle, behavior brittle.

Resumen

La calidad de la mayoría de los productos de metal depende de la condición de sus superficies y del deterioro de estas debido al uso; este deterioro suele ser el factor más importante de la vida útil y el desempeño de los componentes de una máquina. La erosión es una de las causas más destructivas a la que están expuestos los metales. En el presente trabajo, se realizaron pruebas de erosión por impacto de partículas sólidas en acero inoxidable 440C. Se utilizó arena sílica (SiO_2) como erodente (es el abrasivo natural contaminante más común en la corteza terrestre, constituye más del 60%), ensayando cuatro ángulos de impacto a cuatro velocidades de la partícula. Las gráficas de erosión obtenidas, muestran una tendencia al comportamiento frágil. Para determinar la rugosidad y la máxima profundidad de las huellas de erosión se utilizaron escaneos 3D, mostrando que el ángulo de impacto de la máxima pérdida de masa no coincide con el ángulo en el cual ocurre la máxima penetración de la huella de erosión a 5 y 10 psi. Se utilizó microscopia electrónica de barrido para la determinación de los mecanismos de erosión a cada ángulo de impacto ensayado. Estos resultados del comportamiento bajo la erosión fueron comparados con estudios similares, en los cuales el comportamiento bajo la erosión es diferente (en esta investigación la máxima erosión se observó a un ángulo de 60º y en otras investigaciones la máxima erosión se dio a 30º).

Palabras clave: acero inoxidable 440C, erosión, arena sílica SiO_2, ángulo de impacto, comportamiento frágil.

1 Introduction

Stainless steels have numerous applications in different industrial sectors due to its excellent mechanical properties besides its easy forming processes and competitive price (Rodríguez *et al*., 2014), some studies are, AISI-304 (López-Martínez *et al*., 2013) and AISI-410 (Cuevas-Arteaga *et al*.,2019). AISI-440C belongs to the martensitic group because of its transformation from austenite to martensite produced by the quenching from the austenite phase (Aguinaco - Bravo *et al*., 1999), is considered as a high carbon steel with good resistance to deterioration and good mechanical properties.

* *Corresponding author. E-mail*: jose.ibarra@zapopan.tecmm.edu.mx
https://doi.org/10.24275/rmiq/Mat991
issn-e: 2395-8472

Table 1. 440C stainless steel nominal chemical composition.

Element	Wt (%)
C	0.95-1.20
Mn	1.0
Si	1.0
Cr	16.0-18.0
P	0.04
S	0.03
Mo	0.75

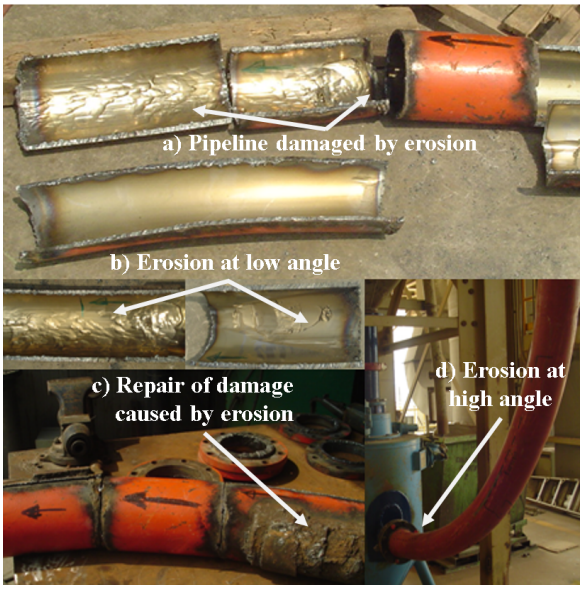

Fig.1. Pipes damaged by silica sand erosion through a pneumatic transportation system.

440C is widely used by industries for manufacturing of pieces such as bearings, guide rings, valve parts, etc. (Smith 1996), as well as mold inserts, industrial knives, food and pharmaceutic industries. Table 1 shows its nominal chemical composition (ASM Handbook vol 1).

Erosion is described as a progressive loss of original material from a solid surface due to mechanical interaction between that surface and a fluid, a multicomponent fluid, or impinging liquid or solid particles (ASTM G76 - 13). The term erosion is also used in other disciplines, for example, soil erosion (Cerda *et al*., 2018, Keesstra *et al*., 2019), erosion by wind action (Feizi *et al*., 2018), but all of them agree that it is a phenomenon of great economic losses due to the deterioration of its surfaces.

Some others examples where erosion phenomena by solid particles occurs are the turbine blades when flying through dust clouds (Stachoviack *et al*., 2005), thermal centrals and pneumatic transportation systems (Sundararajan 1995), fossil energy plants (Adler *et al*., 2001), carbon processing plants (McDonald *et al*., 1994) , etc. Finnie (1995) classified them in 3 categories: fluid flow conditions, particle properties and surface properties. Some of these have been studied by others authors: impact angle (Das *et al*., 2004; Nguyen *et al*., 2014), particle speed (Stevenson *et al*., 1995; Yabuki *et al*., 1999) and particle rotation (Deng *et al*., 2004; Nguyen *et al*. 2015). And among the particle properties (Bousser *et al*., 2013; Murugesh *et al*., 1991): size (Macchini *et al*., 2013; Nguyen *et al*., 2016; Venugopal Reddy *et al*., 1991), shape (Akbarzadeh *et al*., 2012; Feng *et al*., 1999; Laguna-Camacho *et al*., 2015; Naveed *et al*., 2016; Vite-Torres *et al*., 2013), and hardness (Arabnejad *et al*. 2015). Though the influential factors on erosion are many, particle speed and impact angle are considered as determinant in this phenomena. This is the reason because of which the present project is centered in these two variables. Fig. 1 shows images of pneumatic transport system pipes eroded by silica sand where injuries caused by erosion can be observed on the internal surface, Fig. 1a and b, even trespassing totally the pipe wall, so repairing is necessary with the economic consequences on the production system. We can also observe that erosion occurs at different angles of particle-metal, depending on the component geometry Fig. 1 (c) and (d).

When the erosion acts due to solid particles impacts against the material surface, its behavior can be classified as ductile or brittle depending on the angle where the maximum erosion occurs, when the maximum occurs at low angles (20° to 30°) the material has a ductile behavior, if it occurs at angles close to 90°, the material has a brittle behavior (Laguna-Camacho *et al*. 2013; Rateick Jr. *et al*. 2006; E. Rodríguez *et al*., 2009).

Because of wear is one of the causes of deterioration in metallic materials with high economic implications, and 440C stainless steel has shown a wide range of applications, it is important to study its behavior under erosion with the purpose to be considered as an alternative in different applications in which this kind of wear is present. Accordingly, in this work we study the behavior under erosion of 440C stainless steel cryogenically treated, testing four impact angles and four particle speeds.

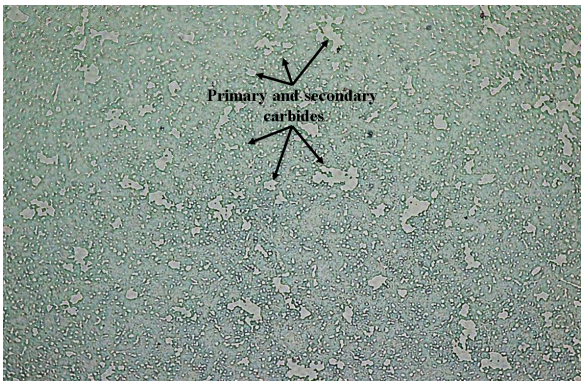

Fig. 2. Microstructure of 440C stainless steel.

2 Materials and methods

2.1 Samples preparation

A 440C stainless steel bar of 7 cm diameter was used to obtain 8 mm thick samples. Their surfaces were prepared until get a roughness inferior to 1.0 microns according to the ASTM G76-13 code for erosion test. All samples were subjected to a quenching heat treatment in order to get a 54 HRC hardness. Afterwards, a cryogenic treatment was applied to the samples with the purpose to transform the retained austenite to martensite (ASM Handbook vol. 4). This treatment consisted of a slow and controlled cooling from room temperature to liquid nitrogen temperature (-196 °C). Subsequently after a holding period of 24 hours, samples were slowly warmed to room temperature (cooling and heating velocities were 2.5 °C/minute). After the cryogenic procedure, a tempering treatment was applied at 250 °C for two hours to release residual stresses (ASM Handbook vol. 4). The microstructure is formed by primary and secondary carbides (islands and particles) on a martensitic matrix, Fig. 2.

2.2 Erosion tests

2.2.1 Erosive media

As an erosive media, mesh 100 silica sand was used, its shape and size are shown in Fig. 3. The amount of sand that was used in each test was determined by preliminary erosion tests. This because low pressure tests required more quantity of erosive media to get a trustable measure of mass loss. The sand loads were between 500 and 4500g.

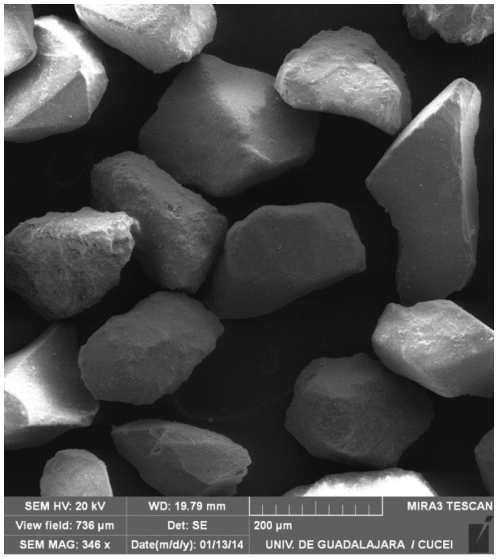

Fig. 3. Silica particles morphology.

The erosion tests were performed according to ASTM G76-13; this code indicates that specimen's surfaces should be conditioned by grounding until get a roughness inferior to 1.0 microns. A sand blast type machine was used and is shown in Fig. 4. The test sequence was as follows:

a) Before and after each test, the samples were immersed in acetone bath and then ultrasonically cleaned during ten minutes. After that the sample was fixed on the sample holder in the wished test angle (15°, 30°, 60°, and 90°).

b) Every selected sand charge was placed inside the charge chamber (see Fig. 4) and fell down by gravity through a tube to the mixing chamber which was under a preset pressure (1, 3, 5 and 10 psi) where the mix of dry air (-40 °C dew point) and sand is generated. The air-sand mix is expelled through the exit nozzle to impact the metallic sample placed on the sample holder. Each test condition was repeated twice. If the tests values difference was above 8%, the test was repeated.

c) Once the sample had been eroded, its mass loss was determined using an analytic balance with 0.1 mg accuracy. After this, the erosion rate was calculated with the Ec. (1).

$$E = \frac{M_R}{M_T} \tag{1}$$

where E is the erosion rate, M_R is the removed material total mass and M_T the erosive particles total mass hitting the surface.

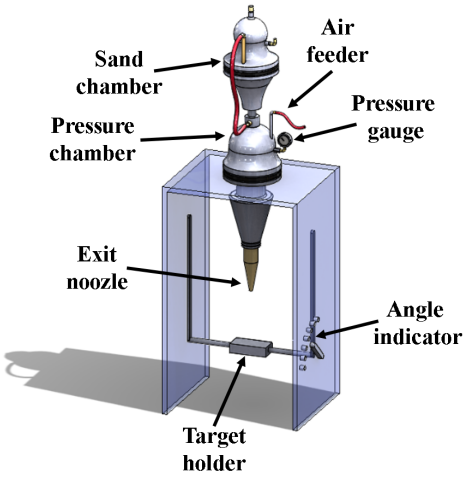

Fig. 4. Scheme of erosive machine sand blast type.

2.2.2 *Particle speed*

The particle speed was determined by the double disk method (Hutchings I.M, 2003), which consists of assembling two separate disks a certain distance, mounted on a machine that contains a rotating shaft Fig. 5. The upper disk has a hole or slot through which erosive particles that will generate two marks in the lower disk are passed. In the idle state of the double disk, an initial mark is made, positioning the hole or slot of the upper disk aligned with the exit nozzle, then the double disk is rotated at a constant speed to generate a second mark, which is outdated to the one made in idle state. The outdated mark with respect to the initial mark it will provide an arc length **S**. Using Eq (2) the particle speed $\mathbf{V_P}$ can be calculated, knowing the angular velocity of the rotation of the disks **U**, the separation distance between the disks **L**, the radius from the axis of rotation to the marks (initial and outdated) **R**, and the arc length generated by the marks **S**.

$$V_P = \frac{2\pi RUL}{S} \tag{2}$$

2.3 *Erosion marks characterization*

To determine roughness and the maximum erosion depth, a 3D mapping of the eroded surface was done using a Dektak 150 surface profiler from veeco with a stylus of 12.5 μm of radius and vision software. Microhardness profiles were done in samples before and after being eroded in order to measure a possible hardness increase due to the plastic deformation generated by the erosion impacts. The indentations were done every 10 μm until a depth of 100 μm. A microhardness tester Future Tech FM-800 and a 10g charge in knoop scale were used.

3 Results and discussion

3.1 *Particle speed*

The double disk method has been an effective method for measuring the particle speed and has been used by various researchers, to mention some (Harsha *et al*., 2008; Rodríguez *et al*., 2009; Rodríguez *et al*. 2007) . For this research, a relationship between particle speed vs blow pressure was obtained and it is shown in Fig. 6, where we can observe that for 1, 3, 5 and 10 psi pressures, we obtain speeds of 38, 58, 66 and 88 m/s respectively. These results are in concordance with the tendency shown by Stevenson *et al*. (1995).

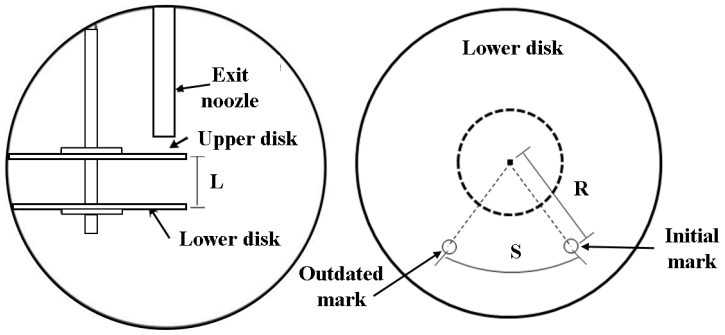

Fig. 5. Scheme of the double disk method.

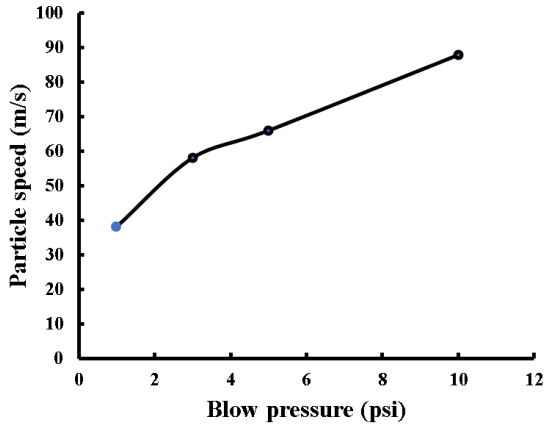

Fig. 6. Speed values of the particle vs blow pressure.

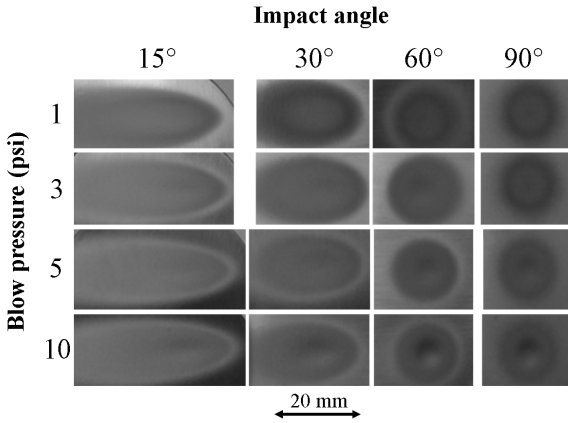

Fig. 7. Erosion marks.

3.2 Erosion marks

Fig. 7 shows the erosion marks generated by the silica sand impact at each angle and pressure tested. We can observe that at 15° and 30° impact angle, an extended mark of elliptical shape is generated taking a larger projected area compared to the marks generated by 60° and 90° that tend to show a circular shape. This is important because at low impact angle, a fixed erodent mass will distribute on a larger sample area, compared to high angle eroded samples. This will influence directly the erosion mark depth, which will be analyzed later.

3.3 Erosion behaviour

Fig. 8 shows the results of the erosion tests at the following impact velocities: 38 m/s (1 psi), 58 m/s (3 psi), 66 m/s (5 psi) and 88 m/s (10 psi) at 15°, 30°, 60° and 90° angles.

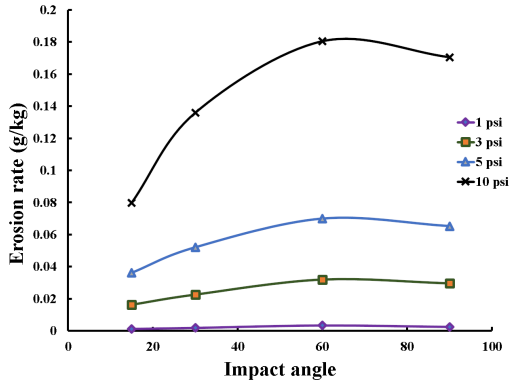

Fig. 8. Erosion values at different impact pressures and angles.

In this Figure it is observed that the maximum of erosion is seen at 60° angle, which shows a behavior with a brittle tendency. Similar results to the shown here are reported by Rodríguez *et al*., (2009) for an AISI 4140 steel and H13 tool steel eroded at 2 blow pressures (10 and 20 psi) where a transition to brittle behavior for both hardened steels at 55 HRC was concluded.

In other research, the authors Rateick Jr. *et al*. (2006); McDonald *et al*. (1994) performed erosion tests in 440C stainless steel but using Al2O3 as the erosive media. They showed that this alloy presents a maximum of wear between 20° and 30° angle, testing similar speeds and angles to the ones of the present research. Another difference consists in the heat treatment applied, Rateick Jr. *et al*. (2006) got a hardness value of 59 HRC and applied a sub-zero treatment (-84 °C) in contrast with this work where a hardness of 54 HRC was obtained and a cryogenic treatment was applied (-196 °C). McDonald *et al*. (1994) only reported that he used hardened 440C SS, but did not specify the obtained hardness nor the heat treatment applied. For the above expressed, we propose that ductile behavior or brittle tendency of this steel depends on the tribological system, influenced mostly by the erosive media characteristics like shape and toughness of the particle.

3.4 Erosion depth

To determine the erosion mark depth, the maximum values pressures were chosen (5 and 10 psi) and 3D mapping were done on 30°, 60° and 90° eroded samples. Fig. 9 shows the erosion surfaces for a 10 psi pressure. This mapping let know maximum penetration of the erosion marks.

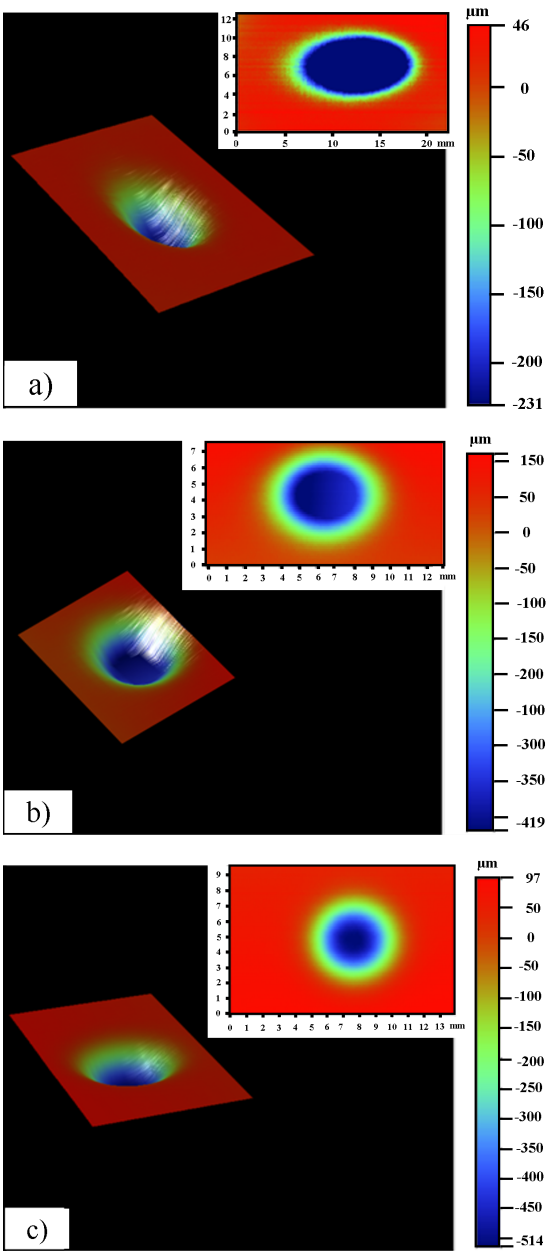

Fig. 9. Erosion mark topography at 10 psi. a) 30°, b) 60° and c) 90°.

The results are shown in Fig. 10, where we observe that the maximum penetration on the sample occurred at 90° angle for both pressure values, which is different from the angle where the maximum erosion occurred at 60° (Fig. 8). This result is very important because in most part of practical applications, thick loss of material is the most critical factor of the component and more mass loss does not imply necessarily more thick loss of the material.

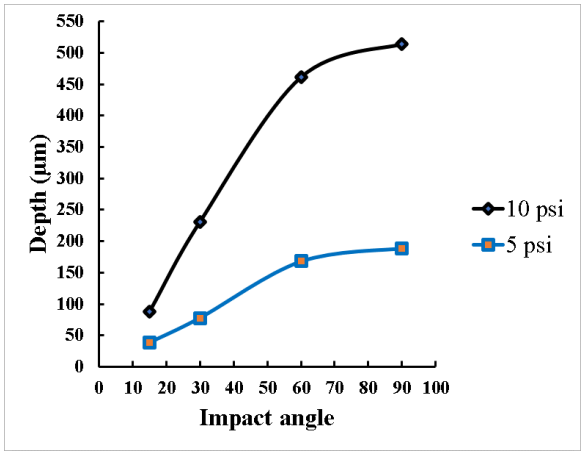

Fig. 10. Maximum depth of the erosion mark.

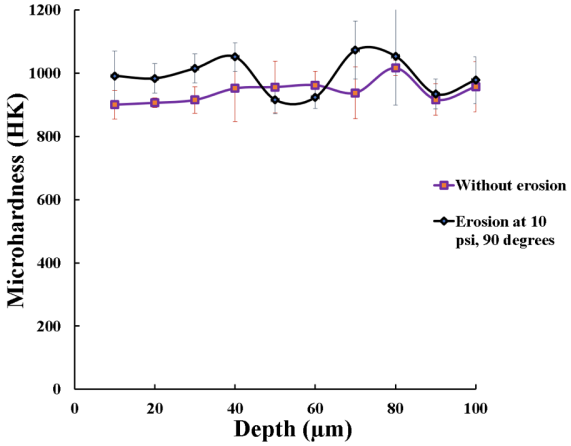

Fig. 11. Microhardness profiles Knoop.

3.5 *Microhardness*

Fig. 11 shows average values of microhardness profiles which do not present a clear alteration in steel hardness attributed to the plastic deformation of the surface. The above is explained by (Rodríguez *et al.*, 2009) who concludes that AISI 4140 and H13 steels highly hardened by heat treatment lose its capacity for an additional hardness increase by plastic deformation, in contrast with the same steel but in annealed state that are more susceptible to harden by deformation and report increases from 103 and 168 HV on the eroded sub-surfaces when they are compared to the matrix hardness.

3.6 *Wear mechanisms*

To determine the way, the material was detached due to the particles impact, only the impact at high speed was analyzed (10 psi, 88 m/s) because at low speed

the way the detachment occurs is similar. Four angles were tested, and we obtained:

a) *15° impact*

Fig. 12 shows that the main cause of detached material for this angle was the cutting action done by the erosive particle generating groove formation with some plastic deformation with the shape of lateral and/or frontal lips (in minor amount), as well as flakes (or chips) at the front of the groove, that are detached by an impact or are susceptible of being detached by successive impacts. This can be explained because the particle speed for this angle has a great tangential component, what makes easy the cutting mechanism and groove formation. The upper left corner inset of Fig. 12, shows a flake about to detach, as well as the groove and lateral lips formation.

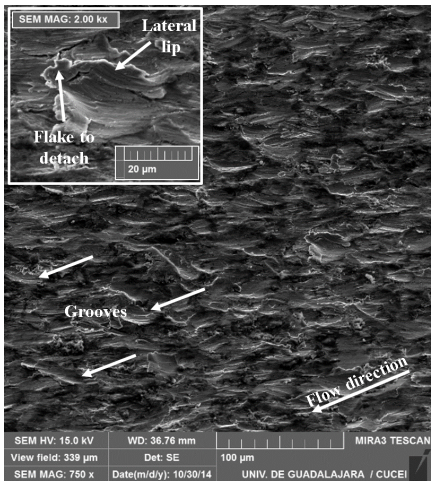

Fig. 12. Eroded surface at 15° angle.

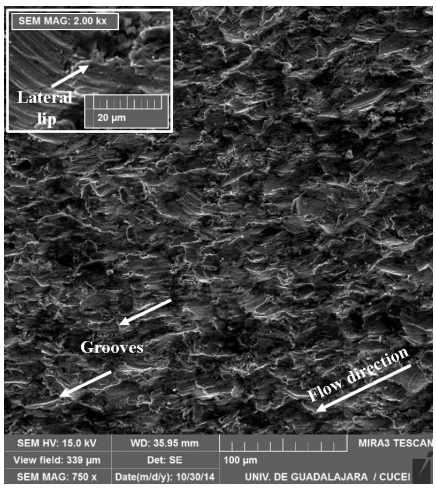

Fig. 13. Eroded surface at 30°.

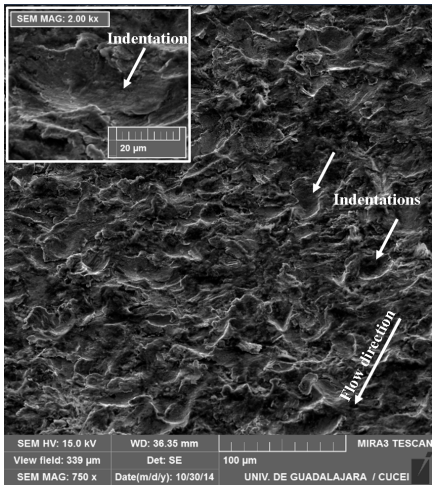

Fig. 14. Eroded surface at 60° angle.

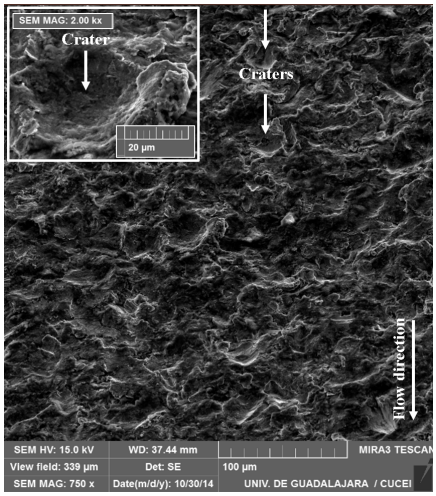

Fig. 15. Eroded surface at 90° angle.

b) *30° impact*

At 30° impact, the plastic deformation has increased showing the shape of lateral and frontal lips, susceptible to be detached by later impacts. In comparison to the 15° erosion, we can observe that the cutting action has decreased but the groove formation (of minor length) keeps on being part of the wear mechanism as it is shown in Fig. 13. Shimizu *et al.* (2011) eroded other steel from the martensitic family (410 stainless steel) and they observed this type of mechanism that was also observed in 403 martensitic stainless steel studied by (Kim *et al.* 1998) using SiC as erodent 100 and 150 μm size, and the particle speed was 40, 70 and 100 m/s.

c) *60° impact*

The erosion surface at 60° is shown in Fig. 14. The grooving mechanism practically disappears; there is a considerable increase in the plastic deformation of the material. We can observe indentation (craters) in a shape that tends to be symmetric. This is explained because, contrary to low angle erosion, now the particle speed has a great normal component to the surface and the tangential component has decreased favoring, in this way, the plastic deformation and the crater formation.

d) *90° impact*

Fig. 15 shows erosion surface at 90°, where the only component of the particle speed is the normal one, and it causes a damage on the surface through craters formation and plastic deformed metal displacement around the impact crater. The successive impacts will cause the later material detachment.

Such behavior was observed in some steels, to mention some: Laguna - Camacho *et al*. (2013) when eroding 304, 316 and 420 stainless steels; Rodríguez *et al*., (2009) in AISI H13 and 4140 steels; Kim *et al*. (1998) in 403 martensitic stainless steel and Rodríguez *et al*. (2007) when eroding AISI 4140 and P20 steels.

Conclusions

The erosion tests results indicate that the maximum erosion is observed at 60° angle, which shows a behavior with a brittle tendency of the material. In other hand, the mapping done on the erosion marks at 30, 60 and 90° impact angles for 5 and 10 psi pressures, indicates that the maximum material loss (at 60° impact) does not coincide with the maximum penetration angle (at 90° impact); this means that the most mass loss does not imply necessarily a mayor material thick loss. In addition, the microhardness profiles did not show any difference between the eroded sub-surface hardness and the rest of the steel hardness; this was attributed to the high hardness obtained by heat treatment that inhibits the hardening capacity by plastic deformation. Finally, the wear mechanisms observed were the next: at 15°, groove formation prevails with little flakes formation and/or detachment , and little plastic deformation ; at 30°, groove formation mechanisms decrease, bit it is still meaningful, besides plastic deformation increases with lateral and frontal lips formation; at 60°, there is no grooves formation and the plastic deformation increase is considerable, leading to the indentation formation with a tendency to be symmetric; at 90°, crater formation prevails surrounded by a big amount of plastic deformation, susceptible to be detached by subsequent impacts.

References

Adler, T. A., Rawers, J. C., Tylczak, J. H. and Hawk. J. A. (2001). Erosive wear of selected materials for fossil energy applications. Conference. December. Knoxville, Tennessee: T*he Fifteenth Annual Conference on Fossil Energy Materials.*

Aguinaco-Bravo, V. J. y Oroño J. (1999). Las partículas elementales básicas como nucleantes de la martensita. *Revista de Metalutgia 35*, 11-16.

Akbarzadeh, E., Elsaadawy, E., Sherik, A. M., Spelt, J. K. and Papini, M. (2012). The solid particle erosion of 12 metals using magnetite erodent. *Wear 282-283*, 40-51. http://dx.doi.org/10.1016/j.wear.2012.01.021

Arabnejad, H., Shirazi, S.A., McLaury, B.S., Subramani, H.J. and Rhyne, L. D. (2015). The effect of erodent particle hardness on the erosion of stainless steel. *Wear 332-333*, 1098-1103. https://doi.org/10.1016/j.wear.2015.01.017

ASM Handbook, Volume 1,(1990). *Properties and Selection: Irons, Steels, and High Performance Alloys.* Materials Park, OH, ASM International.

ASM Handbook, Volume 4,(1991). *Heat Treating*. Materials Park, OH, ASM International.

ASTM Standard, G76-13. (2013). Standard practice for conducting erosion tests by solid particle impingement using gas jets. *International, Contact Astm, and Standard Test Method. 2000.*

Bousser, E., Martinu, L. and Klemberg-Sapieha, J. E. (2013). Effect of erodent properties on the solid particle erosion mechanisms of brittle materials. *Journal of Materials Science 48,* 5543-58.

Cerdá, A., Rodrigo-Comino, J., Giménez-Morera, A., Keesstra, S.D. (2018). Hydrological and erosional impact and farmer's perception on

catch crops and weeds in citrus organic farming in Canyoles river watershed, Eastern Spain. *Agriculture, Ecosystems and Environment 258*, 49-58. https://doi.org/10.1016/j.agee.2018.02.015

Cuevas-Arteaga, C., Clemente, C. M. and Rodríguez. J. A. (2019). Crevices corrosion in cracks of AISI-410 used in steam turbines blades. *Revista Mexicana de Ingeniera Quimica 18*, 13-26. https://doi.org/10.24275/uam/izt/dcbi/revmexingquim/2019v18n1/Cuevas

Das, S., Mondal, D. P. and Sawla. S. (2004). Solid particle erosion of al alloy and al-alloy composites: effect of heat treatment and angle of impingement. *Metallurgical and Materials Transactions A: Physical Metallurgy and Materials Science 35*, 1369-79. https://doi.org/10.1007/s11661-004-0312-4

Deng, T., Bingley, M. S. and Bradley, M. S. A. (2004). The influence of particle rotation on the solid particle erosion rate of metals. *Wear 256*, 1037-49. https://doi.org/10.1016/S0043-1648(03)00536-2

Feizi, Z., Ayoubi, S., Reza Mosaddeghi, M., Asghar Besalatpour, A., Zeraatpisheh, M., Rodrigo-Comino, J. (2018). A wind tunnel experiment to investigate the effect of polyvinyl acetate, biochar, and bentonite on wind erosion control. *Archives of Agronomy and Soil Science 65*, 1049-1062. https://doi.org/10.1080/03650340.2018.1548765

Feng, Z. and Ball, A. (1999). The erosion of four materials using seven erodents - towards an understanding. *Wear 233-235*, 674-84. https://doi.org/10.1016/S0043-1648(99)00176-3

Finnie, I. (1995). Some reflections on the past and future of erosion. *Wear 186-187*,1-10. https://doi.org/10.1016/0043-1648(95)07188-1

Harsha, A. P., and Deepak Kumar Bhaskar. (2008). Solid particle erosion behaviour of ferrous and non-ferrous materials and correlation of erosion data with erosion models. *Materials and Design 29*, 1745-1754. https://doi.org/10.1016/j.matdes.2008.03.016

Hutchings I.M. (2003). *Tribology, Friction and Wear Engineering Materials*. First edition, USA: Elsevier Butterworth-Heinemann.

Keesstra, S. D., Rodrigo-Comino, J., Novara, A., Giménez-Morera, A., Pulido, M., Di Prima, S., Cerda, A. (2019). Straw mulch as a sustainable solution to decrease runoff and erosion in glyphosate-treated clementine plantations in Eastern Spain. An assessment using rainfall simulation experiments. *Catena 174*, 95-103. https://doi.org/10.1016/j.catena.2018.11.007

Kim, J. J., and Park, S. K. (1998). Solid particle erosion of AlSl 403 stainless steel. *Journal of Materials Science Letters 17*, 1503-1506. https://doi.org/10.1023/A:1026403208291

Laguna-Camacho, J. R., Cruz-Mendoza, L. A., Anzelmetti-Zaragoza, J. C., Marquina-Chávez, A., Vite-Torres, M. and Martínez-Trinidad, J (2013). Solid particle erosion on coatings employed to protect die casting molds. *Progress in Organic Coatings 74*, 750-57. http://dx.doi.org/10.1016/j.porgcoat.2011.09.022

Laguna-Camacho, J. R., Hernández-Romero, I., Escalante-Martínez, J. E., Márquez-Vera, C. A., Galván-López, J. L., Méndez-Méndez, J. V., Arzate-Vázquez, I. and Andraca-Adame, J. A. (2015). Erosion wear of AISI 420 stainless steel caused by walnut shell particles. *Transactions of the Indian Institute of Metals 68*, 633-647. https://doi.org/10.1007/s12666-014-0493-5

Lopez-Martínez, E., Hernandez-Morales, J.B., Solorio-Díaz, G., Vergara-Hernandez, H.J., Vazquez-Gómez, O. y Garnica-González, P. (2013). Predicción del perfil de dureza en probetas Jominy de aceros de medio y bajo carbono. *Revista Mexicana de Ingeniería Química 12*, 609 - 619.

Macchini, R.,. Bradley, M. S.A and Deng, T. (2013). Influence of particle size, density, particle concentration on bend erosive wear in pneumatic conveyors. *Wear 303*, 21-29. http://dx.doi.org/10.1016/j.wear.2013.02.014

McDonald, L. G., and Kelley, J. E. (1994). Erosive wear of potential valve materials for coal-conversion plants. U.S. *Department of the Interior, Bureau of Mines, Report of Investigations No. 9490*.

Murugesh, L., and R. O. Scattergood. (1991). Effect of erodent properties on the erosion of alumina. *Journal of Materials Science 26*, 5456-66. https://doi.org/10.1007/BF02403943

Naveed, M., Schlag, H., König, F. and Weiß, S. (2016). Influence of the erodent shape on the erosion behavior of ductile and brittle materials. *Tribology Letters 65*, 1-9. https://doi.org/10.1007/s11249-016-0800-x

Nguyen, Q. B., Nguyenb, V.B., Lim, C. Y. H., Trinh, Q.T., Sankaranarayanan, S., Zhang, Y.W. and Guptaa, M. (2014). Effect of impact angle and testing time on erosion of stainless steel at higher velocities. *Wear 321,* 87-93. https://doi.org/10.1016/j.wear.2014.10.010

Nguyen, V. B., Nguyen, Q. B., Lim, C. Y. H., Zhang, Y. W. y Khoo B.C. (2015). Effect of airborne particle-particle interaction on materials erosion. *Wear 322-323*, 17-31. http://dx.doi.org/10.1016/j.wear.2014.10.014

Nguyen, V. B., Nguyen, Q. B., Zhang, Y. W., Lim, C.Y.H. and Khoo, B.C. (2016). Effect of particle size on erosion characteristics. *Wear 348-349,* 126-37. http://dx.doi.org/10.1016/j.wear.2015.12.003

Rateick Jr., R.G., Karasek, K.R., Cunningham, A.J., Goretta, K.C. and Routbort, J.L. (2006). Solid-particle erosion of tungsten carbide/cobalt cermet and hardened 440C stainless steel-a comparison. *Wear 261*, 773-778. https://doi.org/10.1016/j.wear.2006.01.012

Rodríguez, C., and Biezma, M. V. (2014). Detección de la corrosión por picadura en aceros inoxidables empleando ultrasonidos. *Revista de Metalurgia 50*, 1-11. http://dx.doi.org/10.3989/revmetalm.005

Rodríguez, E., Flores, M., Pérez, A, Mercado-Solis, R.D., González, R., Rodríguez, J. and Valtierra, S. (2009). Erosive wear by silica sand on AISI H13 and 4140 steels. *Wear 267*, 2109-2115. https://doi.org/10.1016/j.wear.2009.08.009

Rodríguez, J., Martinez, D., Perez, A., González, R., Rodríguez, E. and Valtierra, S. (2007). Erosion wear in heat treated tool steels used in core boxes at automotive foundries. *Wear 263*, 301-308. https://doi.org/10.1016/j.wear.2006.12.051

Stachowiack., G.W., Batchelor., A.W. (2005). *Engineering Tribology*. Elsevier Butterworth-Heinemann, ISBN: 9780123977762.

Shimizu, A., Xinba, Y., Ishida, M. and Kato, T. (2011). High temperature erosion characteristics of surface treated SUS410 stainless steel. *Wear 271*, 1349 - 1356. https://doi.org/10.1016/j.wear.2011.01.055

Smith W. F. (1996). Principles of Materials Science and Engineering. Editorial Mcgraw Hill, U.S.A. Stevenson, A. N. J., Hutchings, I. M. (1995). Scaling laws for particle velocity in the gas-blast erosion test. *Wear 181*, 56 - 62. https://doi.org/10.1016/0043-1648(95)90008-X

Sundararajan, G. (1995). The solid particle erosion of metallic materials: the rationalization of the influence of material variables. *Wear 186-187*, 129-144.

Venugopal Reddy, A. and Sundararajan, G. (1991). The influence of grain size on the erosion rate of metals. *Metallurgical Transactions A 18*, 1043-1052. https://doi.org/10.1007/BF03325714

Vite-Torres, M., Laguna-Camacho, J. R., Baldenebro-Castillo, R. E., Gallardo-Hernández E. A., Vera-Cárdenas, E. E., Vite-Torres, J. (2013). Study of solid particle erosion on AISI 420 stainless steel using angular silicon carbide and steel round grit particles. *Wear 301*, 383-89. https://doi.org/10.1016/j.wear.2013.01.071

Yabuki, A., Matsuwaki, K. and Matsumura. M.(1999). Critical impact velocity in the solid particles impact erosion of metallic materials. *Wear 233-235*, 468-75. https://doi.org/10.1016/S0043-1648(99)00170-2